Biochar composite adsorbent for the removal of Cu(II) and Pb(II) from wastewater prepared by the pyrolysis of oil-based drilling cuttings and orange peels

ABSTRACT

Adsorption is a promising method for heavy metal removal from wastewater. How to develop a cost-effective and efficient adsorbent is critical for its practical application. In this study, a biochar composite was developed by using the co-pyrolysis of oil-based drilling cuttings(OBDC) and orange peels (OP), two types of wastes from oil industry and agriculture, respectively, for the adsorption of Cu(II) and Pb(II). The structure, morphology and surface functional groups of the biochar composite from oil-based drilling cuttings and orange peels (ODPR-OB) were investigated by scanning electron microscopy (SEM), energy dispersive spectroscopy (EDS), X-ray diffraction (XRD) and Fourier transform infrared spectroscopy (FTIR). In addition, the adsorption capacity of the ODPR-OB biochar composite for Cu(II) and Pb(II) removal from aqueous solutions under different operating conditions was investigated. The results show that the ODPR-OB biochar composite has a lower contact angle, smaller pore size and higher micropore volume than either oil-based drilling cutting pyrolysis residues(ODPR) or orange-peel biochar(OB), indicating a synergistic effect of co-pyrolysis for an enhanced adsorption. The adsorption capacity of the ODPR-OB biochar composite for Cu(II) and Pb(II) reached 95.11 mg/g and 164.08 mg/g, respectively, which are higher than that of either ODPR or OB, in agreement with the physical characteristics of three types of materials. The adsorption experimental results suggest that the Cu(II) and Pb(II) removal is mainly via surface complexation and electrostatic interaction. Competitive adsorption experiments confirmed that the ODPR-OB biochar composite had a higher adsorption of Pb(II) than of Cu(II), but both Pb(II) and Cu(II) were removed by adsorption satisfactorily. Given the fact both OBDC

and OP are wastes for disposal and there is a synergistic effect from the co-pyrolysis for enhanced adsorption, the ODPR-OB biochar composite has great potential for practical application in terms of Pb(II) and Cu(II) removal from wastewater.

1 Introduction

Heavy metals in industrial wastewater from industrial production processes might pose a serious threat to the environmental ecology if not removed because they could be accumulated and negatively affect the metabolism of living organisms including human beings. Among heavy metal ions, Pb(II) is one of the most dangerous heavy metals, while Cu(II) is a common and mildly toxic[1, 2]. They cannot be degraded by any organisms, and could accumulate in animals by food chain, causing severe damage to gastrointestinal, lung, liver, kidney, and nervous system tissues [3, 4]. Therefore, it is very necessary to remove these pollutants from wastewater.

Different technologies such as chemical precipitation, ion exchange, membrane filtration, solvent extraction, biological removal, and adsorption [5] have been explored to remove heavy metals from wastewater. Among them, Adsorption is widely accepted as a promising technology due to simple process and easy operation[6]. A highly efficient and cost-effective adsorbent is prerequisite for the implementation of adsorption in real-world scenarios. Therefore, extensive studies have been conducted to develop different types of adsorbents. Biochar is becoming one of the most popular adsorption materials accompanying with the development of biofuel production from pyrolysis of biomass wastes. For example, biochars from biomass wastes such as peanut shells[7], orange peel[8] chestnut shells[9], poultry manure[10], bamboo sawdust[11] and other biomass wastes have been studied for heavy metal removal from wastewater. Among these wastes, orange peels are abundant and very common. However, the adsorption capacity of the pristine biochar is limited[12]. Therefore, Modification of biochar to enhance its physicochemical properties has been a potential solution for its use as adsorbents.

Doping minerals is one of modification methods to improve the adsorption capacity of biochar. Suryadi Ismadji et al[13] succeeded in removing ammonia from water with a

bentonite hydrochar composite made from bentonite and cassava peel. Song et al[14] prepared montmorillonite modified biochar for Zn (II) removal from an aqueous solution. Mineral-doped biochar is generally prepared by co-pyrolysis of biomass raw materials and inorganic salts [14]. The doped minerals can thus be dispersed and stabilized in the carbon matrix of biochar [15], tuning the physicochemical properties of the biochar such as pore structure and specific surface area. Meanwhile, the doped minerals can synergistically adsorb different pollutants with the carbon matrix of biochar[16], leading to improved adsorption capacity for most pollutants including heavy metals.

Oil-based drill cuttings (OBDC) are a mixture of drilling fluid and cuttings, composing of various ores and organic matters. After pyrolysis at high temperatures, the organic matter of OBDC is converted into gas and the pyrolysis residues is mainly rich in minerals such has calcite, barite, quartz, etc. It has been found that calcite and barite play an important role in the adsorption of heavy metal ions. Liuyang et al[17] reported a successful removal of Cr (VI) from wastewater by using secondary pyrolytic oil-based cutting pyrolysis residues. This suggests that pyrolyzed OBDC has a good potential for heavy metal ion adsorption, but OBDC pyrolysis residues (ODPR) particles are too small to be recovered easily after adsorption for regeneration. Therefore, we proposed in this study to pyrolyze the mixture of ODPR and OP as a mineral doping method to biochar of OP to enhance both the adsorption capacity of the material and residues recycling to improves the application prospect of wastes in environmental remediation. In this study, biochar composites prepared from the mixed orange peel and OPDR were used as adsorbents for the removal of Cu(II) and Pb(II) from aqueous solutions. The effects of the ratio of two raw materials on adsorption capacity of Cu(II) and Pb(II) were investigated for the optimal mixing ratio between ODPR and OP. The adsorption behavior and adsorption mechanism of the ODPR-OB composites were studied in detail.

2 Materials and methods

2.1 Materials

Oil-based drill cuttings (OBDC) were taken from an oil and gas exploration platform

in Changning, Sichuan Province. Orange peels(OP) were obtained from a vegetable market near Southwest Petroleum University in Sichuan Province, China, OP was washed with deionized water and then air-dried at 60 °C. Subsequently, the dried OP was mechanically shredded for biochar preparation. Chemical reagents such as copper nitrate ($Cu(NO_3)_2$; AR), lead nitrate ($Pb(NO_3)_2$; AR), sodium hydroxide (NaOH; AR), and hydrochloric acid (HCl; AR) were purchased from Cologne, Chengdu. All solutions were prepared by using deionized water.

2.2 Preparation of ODPR-OB composite

First, 30 g of the OBDC was pyrolyzed at 500 °C with a heating rate of 20 °C/min in an inert atmosphere of N_2, after 30-min pyrolysis at 500 °C, the tube furnace was cooled to room temperature 25°C to obtain ODPR[18]. The ODPR was washed three times with pure water to remove soluble impurities, and then dried in an oven at 80 °C. Then, 10 g-20 g of the ODPR was mixed with 500mL of pure water, and stirred for 30min to obtain a stable ODPR suspension. Then 10 g-20 g of OP mixed well with ODPR suspensions with a certain range of ratios and stirred for 2 h. Finally, the mixture was filtered, and dried at 80 °C in the oven, followed by pyrolysis in a tube furnace. The details were as follows: (i) OP and ODPR in different ratios (0:1, 1:1, 1:2, 2:1, 1:0) were mixed each time. (ii) Different types of ODPR-OB were obtained by pyrolysis with the above method. The adsorption capacities of the ODPR-OBcomposites prepared at three different mixing ratios for Cu(II) and Pb(II) adsorption were compared, and the one with the best performance was selected for subsequent experiments. In addition, the ODPR and the OB obtained by OP, were used as controls to study the synergetic effects of mixing two types of materials for adsorption enhancement.

2.3 Characterization methods

Scanning electron microscopy (Zeiss Supra 55, Germany) was used to observe the microstructure of OB, ODPR and ODPR-OB, respectively. An energy spectrometer (Oxford Company, British) was used to determine the composition element content on the surface of the three materials. The crystal structures of the three materials were obtained by X-ray powder diffraction (X'Pert, PROMPD). Fourier transform infrared spectroscopy (WQF-520, Beijing Rayleigh) was used to detect chemical functional

groups on the surface of three materials. The contact angles which reflects the wettability of aqueous solution on material surface were measured by using contact Angle measuring instrument (DSA100, Germany). The nitrogen adsorption isotherms of the materials were plotted using an automatic specific surface area and porosity analyzer (Micromeritics APSP 2460, USA). Meanwhile, the corresponding specific surface area (BET), pore size and pore volume of the material were obtained.

2.4 Cu(II) and Pb(II) adsorption experiments

Cu(II) and Pb(II) solutions were prepared from copper nitrate and lead nitrate. Copper nitrate ($Cu(NO_3)_2$) and lead nitrate ($Pb(NO_3)_2$) were dissolved in deionized water, respectively, to prepare stock solutions with a concentration of 5000 mg/L of Cu(II) and Pb(II), respectively. stock solutions were diluted to appropriate concentrations according to specific experimental requirements. The three adsorption materials, OB, ODPR and ODPR-OB, were added to 50 mL of Cu(II) and Pb(II) solution with a specific concentration (20-350 mg/L) at different doses (0.2-1.2 g/L). The solution with the addition of adsorbents were shaken on a shaker at 200 rpm according to the prescribed time(0-24 h). The effects of adsorbent dosage, adsorption contact time, initial concentrations of Cu(II) and Pb(II) solutions, and different initial pH values on the removal of Cu(II) and Pb(II) were investigated. After the adsorption experiment, the adsorbent was removed by a filtration with a 0.45 μm membrane filter, and the filtrate was collected immediately. The concentrations of Cu(II) and Pb(II) were determined with an atomic absorption spectrophotometer (SP-3500AA, Shanghai). The Cu(II) and Pb(II) adsorption capacities were calculated using the following formula (1):

$$q_e = \frac{(C_0 - C_e)V}{m} \quad (1)$$

where q_e (mg/g) was the equilibrium adsorption capacity, C_e (mg/L) was the concentration of Cu(II) and Pb(II) in the equilibrium solution, and C_0 (mg/L) was the Cu(II) and Pb(II) in the initial solution. V(L) was the solution volume and m(g) was the adsorbent mass.

In addition, the competitive adsorption experiments of Cu (II) and Pb (II) were performed by OB, ODPR and ODPR-OB at different pH values. The AIC model was used for statistical analysis to compare the selective adsorption capacity of Cu (II) and

Pb (II). The formula is as follows:

$$k_d = \frac{C_0 - C_e}{C_e} \times \frac{V}{g} \quad (2)$$

$$\alpha = \frac{k_d(a)}{k_d(b)} \quad (3)$$

Where C_0 was the initial concentration of Cu(II) or Pb(II) in the solution at the equilibrium, C_e (mg/L) was the concentration of Cu(II) or Pb(II) in the solution at the equilibrium, V was the volume of solution, g was the amount of adsorbent, $K_d(a)$ and $K_d(b)$ was the selectivity index of Cu(II) or Pb(II), α was the selectivity coefficient of a specific metal ion. The higher the α value, the greater the selectivity of the adsorbent to the target ion.

2.5 Adsorption isotherm and kinetics

2.5.1 Isotherm

Langmuir and Freundlich isothermal models were used to fit the experimental data. Langmuir equation[19] could be expressed as (4):

$$q_e = \frac{q_m K_L C_e}{1 + K_L C_e} \quad (4)$$

Where q_e (mg/g) was the equilibrium adsorption capacity, C_e (mg/L) was the concentration of Cu(II) or Pb(II) in the solution at the equilibrium, q_m (mg/g) was the theoretical adsorption capacity of adsorbent and K_L (L/mg) was the affinity coefficient. Freundlich equation[20] could be expressed as (5):

$$q_e = K_F C_e^{1/n} \quad (5)$$

Where K_F was Freundlich constant (L/mg) and 1/n was the heterogeneity factor.

2.5.2 Kinetic

Several commonly used dynamics models such as Pseudo-first-order kinetic, pseudo-second-order, The Elovich model and Intraparticle diffusion kinetic model were used to fit the experimental data. The Pseudo-first-order kinetic equations[21] was shown in formula (5):

$$\ln(q_e - q_t) = \ln q_e - k_1 \times t \quad (5)$$

Where q_e and q_t were the adsorption capacities (mg/g) at equilibrium and time t, respectively. k_1 was the pseudo-first order constant.

The Pseudo-second-order kinetic equation[22] was shown in formula (6):

$$\frac{t}{q_t} = \frac{1}{k_2 \times q_e^{\ 2}} + \frac{t}{q_e} \tag{6}$$

Where k_2 were the pseudo-second-order constant.

The Elovich model[23] was shown in formula (7):

$$q_t = \frac{\ln(\alpha \times \beta)}{\beta} + \frac{\ln(t)}{\beta} \tag{7}$$

Where α was the Elovich model constant, β reflect increased surface coverage of adsorbents.

The Intraparticle diffusion kinetic models[24] was shown in formula (8):

$$q_t = k \times t^{0.5} + C \tag{8}$$

Where k was the Intraparticle diffusion kinetic model constant, C was related to the thickness and boundary layer of adsorbent.

3 Results and discussion

3.1 Characterization

The SEM image of OB, ODPR and ODPR-OB were shown in Fig. 1. It can be observed that OB had a clearer pore structure and more folds of channel surface, which could provide better conditions for OPDR doping (Fig. 1a, b). The surface of OPDR was layered, with serious particle accumulation and aggregation, and no obvious pores and channels were observed (Fig. 1c, d). ODPR-OB (Fig. 1e, f) retained the porous structure of OB, and the ODPR-doped composites were more dispersed than ODPR particles alone. This means that the exposure of active sites became higher, which was more favorable for adsorption.

The element contents of the three sorbents were shown in Fig. 1g-i. As seen, the surface of OB mainly contains C element and there were few minerals. This is mainly determined by the organic nature of OP, and fixed carbon was the main element in the OB. On the contrary, OBDC contained minerals and oils, resulting in main elements of C, O, K and Ca and multiple other elements such as Mg, Al, Si, S, Fe and Ba. Although C is the main element in both OB and ODPR, C content in ODPR was much lower than

that of OB due to the dominance of minerals rather than oil in OBDC as shown in Fig. 1h. After mixing, ODPR-OB composite showed the mixture of elements of ODPR and OB with high both C and other metal element contents, demonstrating a successful doping of minerals from ODPR on the surface of OB for potential enhancement of adsorption active sites.

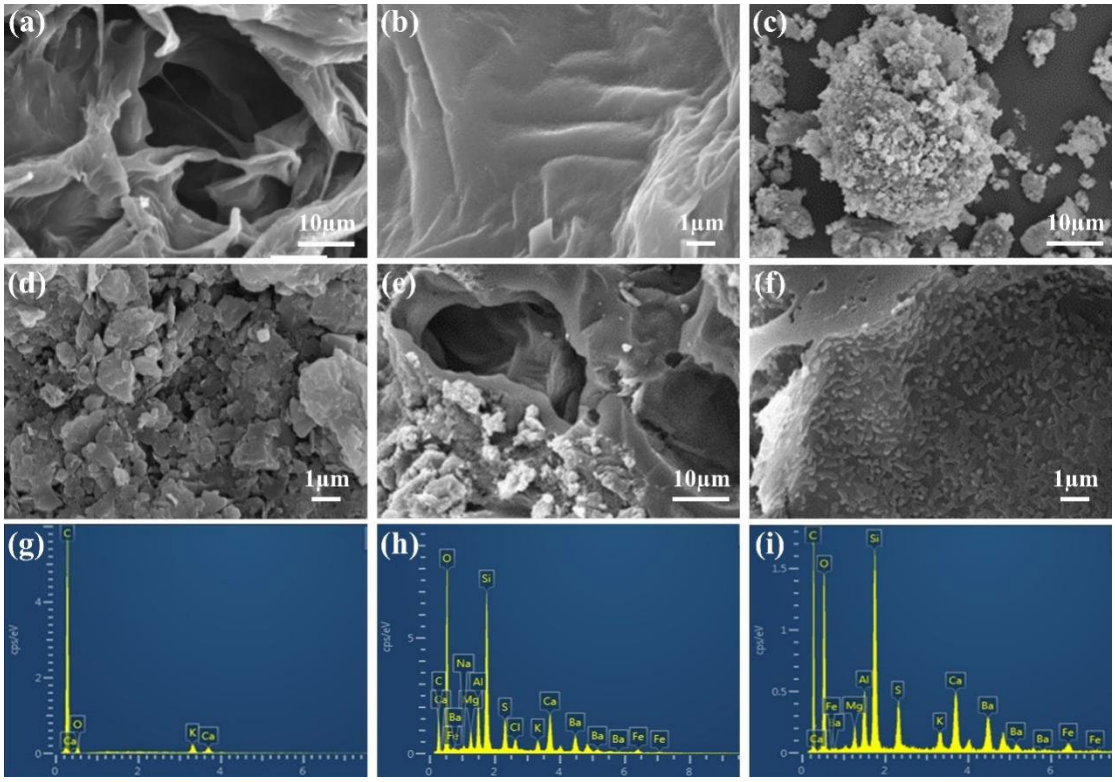

Fig. 1. SEM images of OB (a, b), ODPR (c, d) and ODPR-OB (e, f) at different magnifications. EDS images of OB (g), ODPR (h) and ODPR-OB (i)

The XRD spectra of OB, ODPR and ODPR-OB were shown in Fig. 2a. OB had obvious bulges at 2θ=20 ° and 2θ=40 °, a typical range of the diffraction of graphite crystals which was related to the graphitization of the precursor at high temperature pyrolysis stage [25]. The composition of ODPR looked like complex mixture. Crystals such as quartz[26], calcite[27], hematite[28], pyrite[29] and barite[30] were found in Fig 2a, these mineral oxides can co-precipitate with heavy metal ions and complex with inner spheres[31]. The above-mentioned material diffraction peaks also appear in ODPR-OB. And a similar bulge to OB could also be observed at 2θ=20 ° and 2θ=40 ° of ODPR-OB. This indicated that ODPR was successfully doped in OB to get the ODPR-OB composite. Wu, C., et al [18] also reported a similar phenomenon.

To understand the functional groups on the surface of three types of adsorbent, FTIR was used as shown in Fig. 2b. The absorption peaks of ODPR and ODPR-OB at 3430 cm^{-1} indicate the presence of hydroxyl (-OH) on the surface of the adsorbent [32]; the absorption peak of OB and ODPR-OB at 2928 cm^{-1} corresponds to the -CH bond in the stretching vibrations of -CH, $-CH_2$ and $-CH_3$; The stretching vibration band of OB at 1569 cm^{-1} belongs to the C=O bond in the carboxyl group or ester group (-COOH,-$COOCH_3$);The absorption peaks of OB and ODPR at 1436 cm^{-1} corresponds to the stretching vibration peak of the C=O bond in the ionized carboxyl group (-COO-) on OB and the stretching vibration peak of hydrated calcium aluminate or calcium carbonate on ODPR. The absorption peaks ODPR and ODPR-OB at 1100 cm^{-1} and 1000 cm^{-1} corresponds to the stretching vibration peaks of sulfate and silicate [33]. These results indicated that ODPR-OB almost retained all functional groups of OB and ODPR. These results indicated that ODPR-OB retains all functional groups on ODPR and OB. The oxygen-containing functional group which played an important role in the adsorption of heavy metal ions is the main functional group. Lu[34] also reported that metals can produce surface complexation with carboxyl and hydroxyl functional groups.

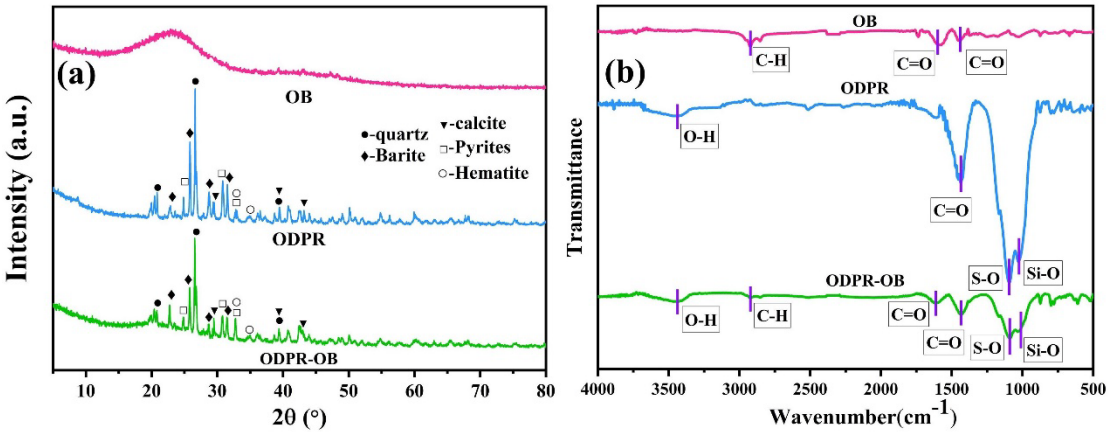

Fig. 2. XRD images(a) and FTIR spectra(b) of OB, ODPR and ODPR-OB.

To gain insight further into the surface properties and porous structure of the samples, we measured contact angle and conducted N_2 adsorption-desorption experiments. As shown in Fig. 3, the three materials all exhibit mixed curves of type II and type IV isotherms[35], which reflected the adsorbent has the characteristic of mesoporous and macroporous. Type II isotherms were usually used to describe macroporous adsorption

and monolayer-multilayer adsorption, while type IV isotherms are usually used to represent multilayer adsorption and capillary condensation. As the relative pressure increases, a hysteresis loop was observed due to capillary condensation. The hysteresis loops of the three adsorbents are all H3-type hysteresis loops[35], which suggest that the pores might be flat slits, fissures, or have wedge-shaped structures.

The angle of contact, specific surface area (BET), pore size and pore volume of the three materials were shown in Table 1, from which it can be seen that the ODPR-OB is not a simple mixture of ODPR and OP. Certain reactions could occur between OBDC and OP during the pyrolysis and thus change the properties of ODPR-OB composites. For example, the contact angle of ODPR-OB composite was the smallest compared with ODPR or OB. The smaller contact angle indicates higher water affinity, facilitating the adsorption of heavy metal ions in an aqueous solution. The specific surface area of ODPR-OB composite was similar to that of ODPR, but significantly higher than that of OB, and the pore volume is the largest among the three, and the pore size is the smallest among the three. This indicated that ODPR has been successfully doped on the surface and pores of OB[36], making the pore size smaller. However, as the doping process was the secondary pyrolysis of OBDC[17], more pore sizes were generated in the composite, resulting in the increase of pore volume.

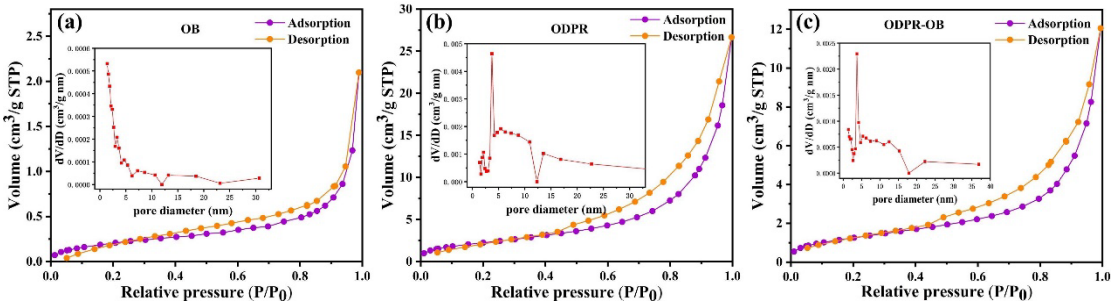

Fig. 3 N_2 adsorption and desorption isotherm of OB(a), ODPR(b) and ODPR-OB(c)

Table 1 Specific surface area and contact angle of OB, OPDR and ODPR-OB

Adsorbent	OB	ODPR	ODPR-OB
Contact angle	56.81°	40.23°	29.9°
Specific surface area（m^2/g）	0.7157	8.435	7.726
Micropore volume（cc/g）	3.245×10^{-3}	4.123×10^{-2}	4.864×10^{-2}
Pore size（nm）	18.14	19.55	15.78

3.2 Removal of Cu(II) and Pb(II) from an aqueous solution with ODPR-OB as adsorbents

3.2.1 Optimizing ODPR/OP ratios in the ODPR-OB composite for the highest Cu(II) and Pb(II) adsorption

The adsorption capacity of ODPR-OB composite with different OBDC/OP ratios (0:1, 1:2, 1:1, 2:1, 1:0) for Cu(II) and Pb(II) was shown in Fig. 4. The ODPR-OB composite with ratio of 1:1 ODPR and OP had the highest adsorption capacity for both Cu(II) and Pb(II). This phenomenon might be because that the different ratios of ODPR and OP, leaded to the different changes of adsorption sites. When there was too much ODPR, the ODPR would seriously accumulate on the surface or in the pores of OB. While there was too little ODPR, it might lead to insufficient adsorption sites. Therefore, the ODPR-OB composite with 1:1 ODPR and OP ratio was selected for further adsorption experiments to study the adsorption performance for Cu(II) and Pb(II).

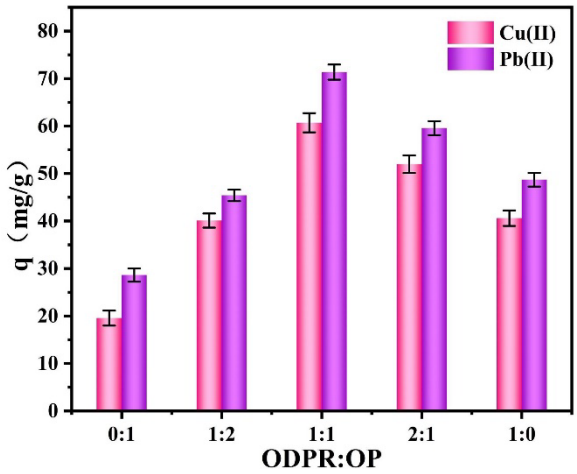

Fig. 4 Adsorption of Cu(II) and Pb(II) by ODPR-OB composite with Different ODPR/OP ratios

3.2.2 Effect of dosage of adsorbents on Cu(II) and Pb(II) adsorption

The dosage of adsorbent was set in a range of 200-1200 mg/L. As shown in Fig. 5, In this experiment, the removal rates of Cu(II) and Pb(II) by ODPR-OB composite were much higher than ODPR or OB. This again strongly proved that ODPR-OB composite was not a simple mixture of ODPR and OP, which agreed with the physical characteristics of each type of adsorbent shown in Table 1. Instead, the chemical reaction between ODPR and OP could occur during pyrolysis to create more adsorption sites for a significantly improved Cu(II) and Pb(II) adsorption[37]. In addition, When

the ODPR-OB dosage increased to 600mg/L, the removal rates of Cu(II) and Pb(II) increased rapidly to 43.94 % and 75.52 %. When the ODPR-OB dosage increased from 600mg/L to 1200mg/L, the removal rates of Cu(II) and Pb(II) ions also increased slowly to 61.99 % and 95.17 %. Although Cu(II) and Pb(II) removal rates were higher at the higher dosage, the driving force of adsorption decreased significantly with the increase in the number of excess adsorption sites. From qt, it can be seen that q_t relatively stabilized at a dosage of 1000 mg/L above, thus, in practice, 1000 mg/L could be selected as an optimal dosage by considering both Cu(II) and Pb(II) removal rate and economic benefit.

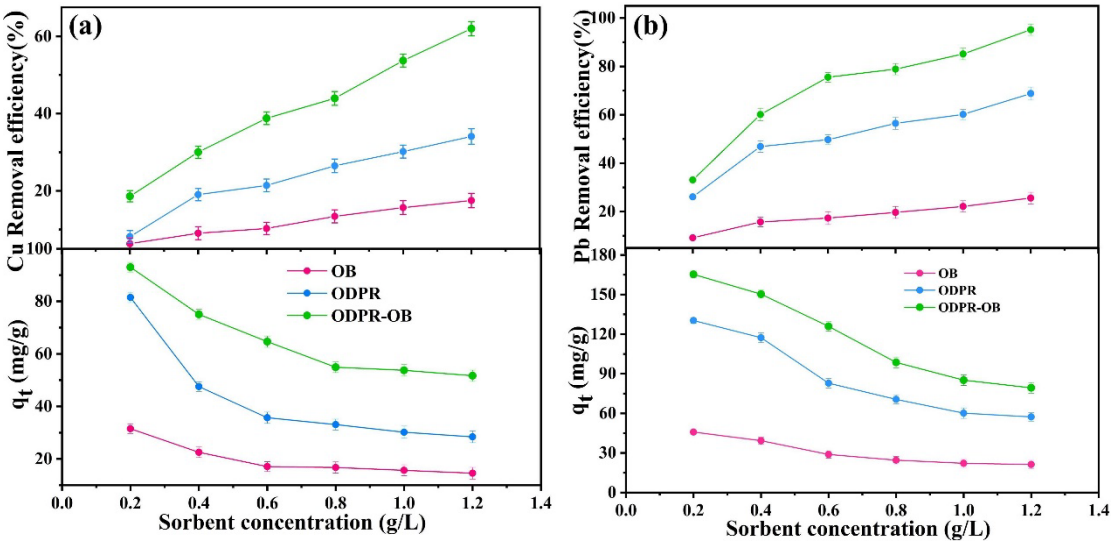

Fig. 5. Effect of adsorbent dosage on removal of Cu (a) and Pb (b)

3.2.3 The effect of adsorption contact time

The contact times for adsorption of Cu(II) and Pb(II) were preset at 0, 0.5, 1, 2, 4, 8, 12, 20 and 24 h, respectively, with initial concentrations of adsorbent of 1000 mg/L and Cu(II) and Pb(II) ions of 250 mg/L. As shown in Fig. 6, the adsorption of Cu(II) and Pb(II) by ODPR-OB composite reached equilibrium within 12 h, similar to ODPR or OB. This Indicated that the co-pyrolysis of ODPR and OP did not affect the equilibrium contact time of coke composites, but greatly increases the adsorption capacity of Cu(II) and Pb(II).

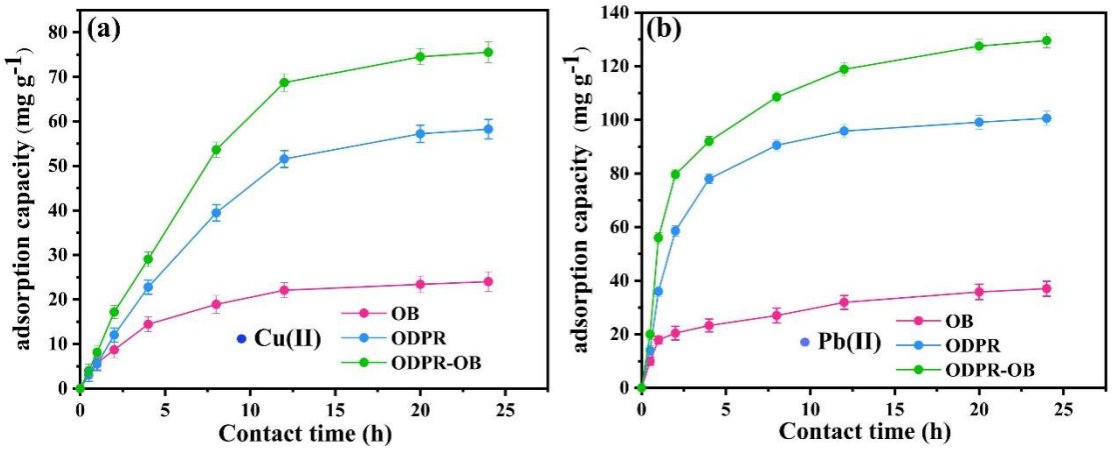

Fig. 6. the contact time for reaching adsorption equilibrium of Cu(II)(a) and Pb(II)(b) by OB, ODPR, and ODPR-OB .

3.2.4 Effect of initial Cu(II) and Pb(II) concentrations on adsorption efficiency capacity of adsorbents

Fig. 7 shows the adsorption capacity of adsorbents at different initial concentrations of Cu(II) and Pb(II). With the increase in initial Cu(II) and Pb(II) concentration, the adsorption capacity of ODPR-OB showed a similar trend with ODPR with higher adsorption capacity at higher initial Cu(II) and Pb(II) concentration, but always with higher adsorption capacity at different metal concentrations. In addition, with the increase of heavy metal ion concentration, the adsorption capacity of ODPR-OB first increased rapidly and then gradually stabilized. These results might indicate that Cu(II) and Pb(II) could first diffuse on the surface of the adsorbent, resulting in a rapid increase in adsorption capacity. Similar results were reported by other researchers[38]. With the increase in the concentration of Cu(II) and Pb(II), it could be speculated that the activation sites on the surface of adsorbents for adsorption became saturated[33]. the further adsorption is actually due to intra-particle diffusion[39]. Based on this, surface adsorption sites in ODPR-OB composite should be more than ODPR although its surface area is slightly smaller than ODPR as shown in Table 1. This further proved that ODPR and OP are not simply mixed, but chemically react to produce more adsorption sites.

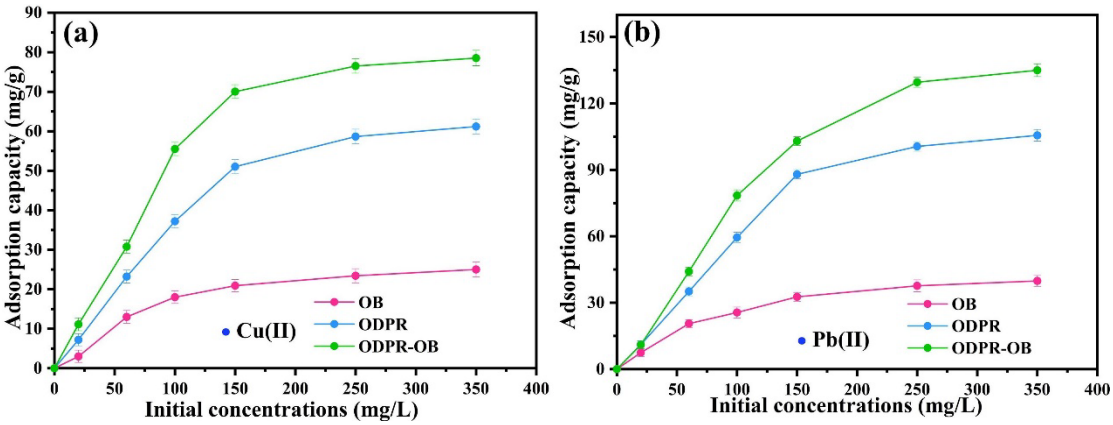

Fig. 7. The effect of the initial Cu (a) and Pb (b) concentrations on the adsorption capacity by OP, ODPR and ODPR-OB

3.2.5 Effect of pH on Cu(II) and Pb(II) adsorption

pH in solution could affect the protonation degree of adsorption sites of adsorbents, the chemical properties and morphology of Cu(II) and Pb(II) in the solution. All these factors would affect the adsorption efficiency of Cu(II) and Pb(II) by adsorbents. In this study, pH of the solutions with an initial Cu(II) and Pb(II) concentration of 100 mg/L was preset as 2,3,4,5 and the natural pH value, respectively, to study the effects of pH. The initial pHs of the solutions were adjusted by 0.1 M NaOH and HCl. It is found from Fig. 8 that an increase in pH from 2 to the natural pH value was favorable to the adsorption of Cu(II) and Pb(II) by all three types of adsorbents. The increasing rates by OB, ODPR, ODPR-OB adsorbents were 19.27%, 35.13%, 45.89% for Cu(II), respectively, and 20.79%, 55.19%, 72.55% for Pb(II), respectively. These results suggest that the existence of excess hydrogen ions at lower pHs resulted in intensive competition between hydrogen ions (H^+ or H_3O^+) and Cu(II) and Pb(II) on the adsorption sites of adsorbents, and thus reduced the adsorption of Cu(II) and Pb(II) by adsorbents[40]. With the increase in pH, the competition of H^+ with other cations was gradually weakened, and the adsorption capacity of the adsorbent was gradually more dependent on the number of adsorption sites on the surface of the adsorbent, such as the number of functional groups and negative charges on the surface of the adsorbent [41]. It was observed that the adsorption capacity of Cu(II) and Pb(II) by ODPR-OB increased with the increase of pH, and the increase was the largest among the three adsorbents. This indicated that the ODPR-OB composite possesses more surface

functional groups and negative charges as adsorption sites for a better adsorption effect. These results might suggest that the adsorption of Cu(II) and Pb(II) by ODPR-OB composite could be mainly via surface complexation and electrostatic adsorption.

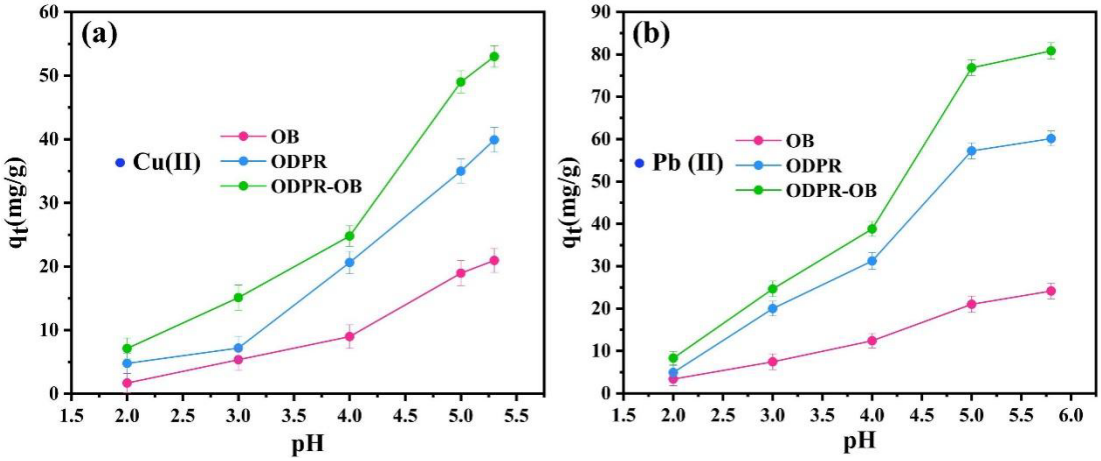

Fig. 8. Effect of pH of solutions on the adsorption of Cu(II) (a) and Pb(II) (b)

3.3 Adsorption kinetics and isotherm of adsorbents

3.3.1 Adsorption Kinetics

The experimental adsorption data fitting curves by different kinetic modules and specific kinetic model parameters were shown in Fig. 9, Fig. 10 and Table 2. By comparing R^2 in Table 2, it can be seen that the pseudo-second-order kinetic model fitted Cu(II) and Pb(II) adsorption by different adsorbents better than other kinetic models with the fitted R^2 close to 1. Therefore, the adsorption process of Cu(II) and Pb(II) by all three types of adsorbents can be described based on the pseudo-second-order adsorption kinetic model. According to the fitting data of the intraparticle diffusion model, the adsorption processes of Cu(II) and Pb(II) for the three materials were similar, and they were not controlled by the diffusion process, but consist of three processes described below. In the first stage ($t^{0.5} \leq 15$), metal ions diffuse to the outer surface of the adsorbent through the solution, and instantaneous adsorption occurs, and the adsorption capacity of the adsorbent increases sharply. In the second stage ($15 \leq t^{0.5} \leq 35$), the metal ions diffuse from the adsorbent surface to the adsorption site, and the adsorption rate slows down. In the third stage ($t^{0.5} \geq 35$), the metal ions were slowly transferred from the macropores to the micropores of the adsorbent, and the

adsorption rate was the slowest among the three stages.

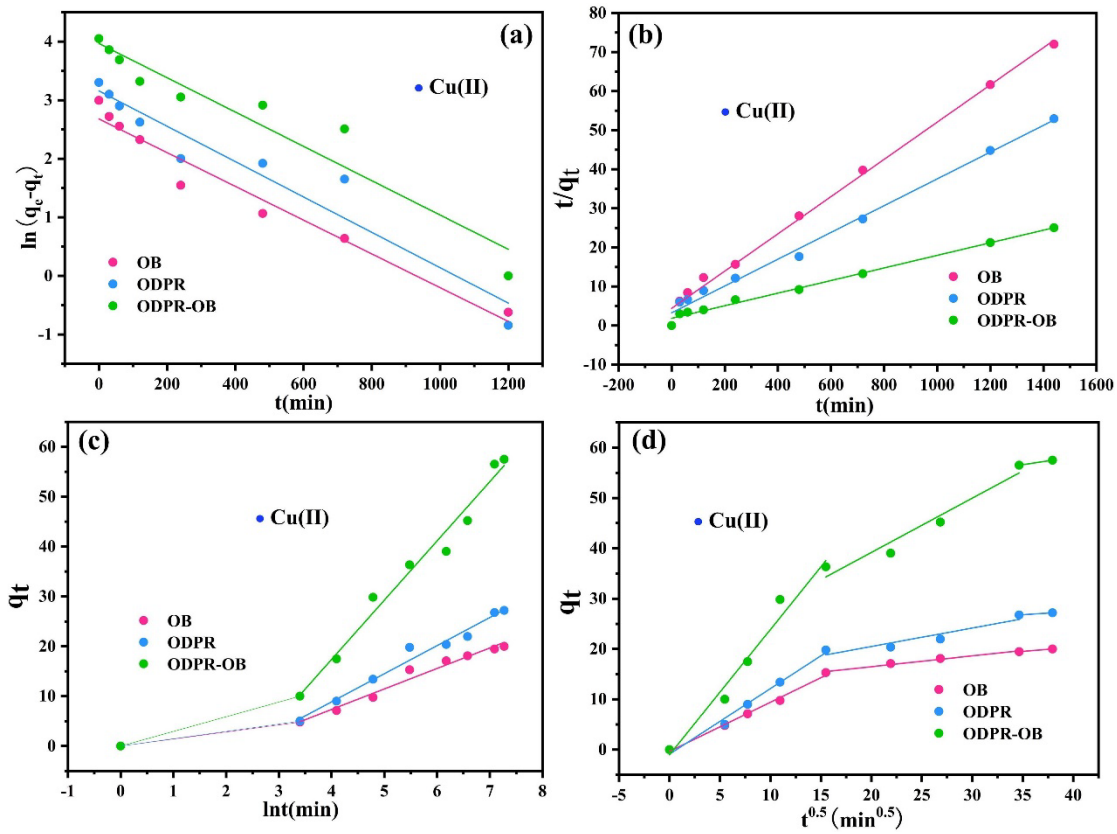

Fig. 9. Fitting of Cu(II) adsorption data by Pseudo-first-order, Pseudo-second-order , Elovich model and Intraparticle diffusion kinetic models of (a-d) for adsorption by OB, ODPR and ODPR-OB, respecitviley.

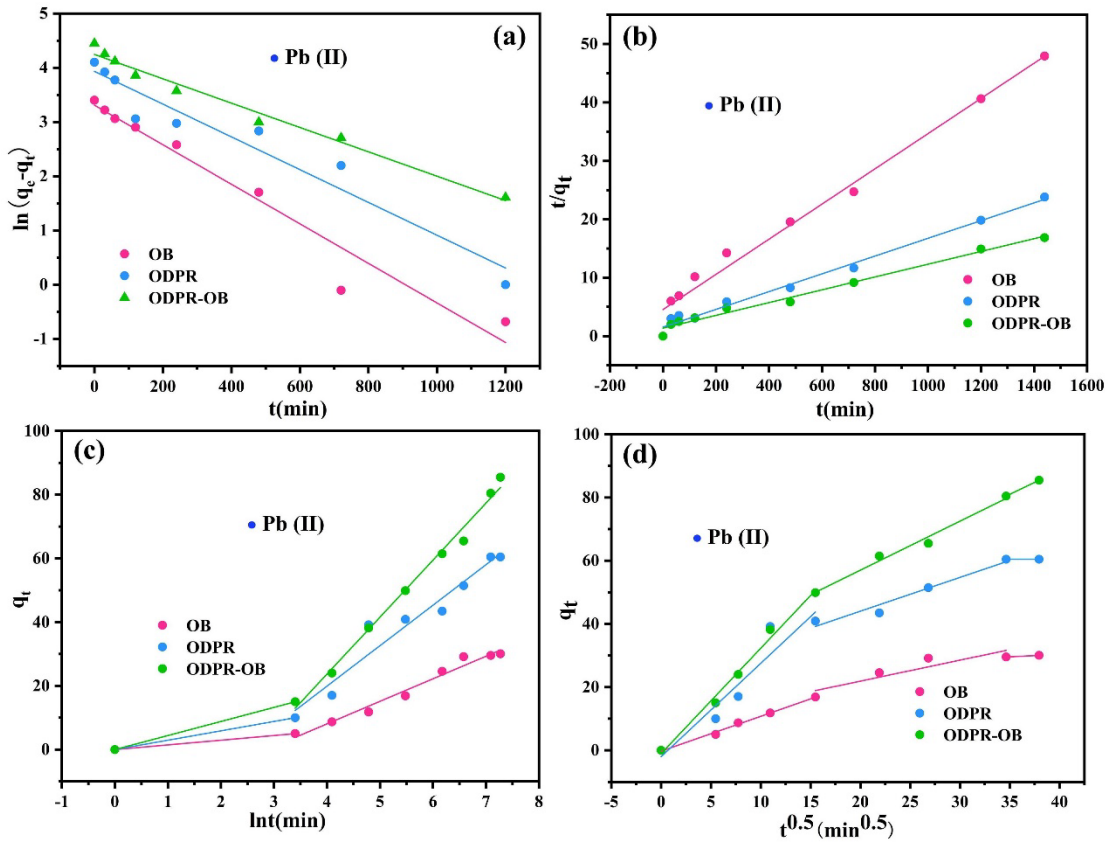

Fig. 10. Fitting of Pb(II) adsorption data by Pseudo-first-order, Pseudo-second-order , Elovich model and Intraparticle diffusion kinetic models (a-d) for adsorption by OB, ODPR and OPDR-OB, respecitviley.

Table 2 Experimentally determined kinetic model parameters for the Cu(II) and Pb(II) adsorption by OB, ODPR, and ODPR-OB

kinetic equations	Parameters	Cu(II)			Pb(II)		
		OB	ODPR	ODPR-OB	OB	ODPR	ODPR-OB
Pseudo-first-order	R^2	0.9576	0.9165	0.9094	0.9451	0.9269	0.9784
	k_1	2.88×10^{-3}	3.02×10^{-3}	2.93×10^{-3}	3.65×10^{-3}	3.02×10^{-3}	2.24×10^{-3}
	q_e	14.589	23.531	52.919	27.371	51.090	69.751
Pseudo-second-order	R^2	0.9938	0.9903	0.9900	0.9816	0.9867	0.9839
	k_2	5.15×10^{-4}	3.58×10^{-4}	1.40×10^{-4}	1.72×10^{-4}	1.46×10^{-4}	8.04×10^{-5}
	q_e	20.982	29.189	62.035	35.714	66.667	95.238
Elovich model	R^2	0.9155	0.8991	0.8878	0.8487	0.8759	0.8821
	A	1.2405	1.4555	2.8186	1.2887	3.2638	3.8033
	B	0.3300	0.2491	0.1204	0.2139	0.1106	0.0819
Intraparticle diffusion	R^2	0.8696	0.9019	0.9331	0.9297	0.8688	0.9569
	K	0.5119	0.6943	1.4655	0.8398	1.5565	2.1852
	C	3.2474	3.5262	6.2229	2.2659	8.0367	7.5680

3.3.2 Adsorption isotherm

To further explore the adsorption mechanism of Cu(II) and Pb(II) by the three adsorbents, the experimental data were fitted by Langmuir and Freundlich, two commonly used isotherm models. The fitting results are shown in Fig. 11, and the fitting parameters are shown in Table 3. The correlation coefficient R^2 suggests that the adsorption behaviors of Cu(II) and Pb(II) by three types of adsorbents were better in line with the Langmuir model than Freundlich. The maximum adsorption capacities of OB, ODPR and ODPR-OB adsorbents for Cu(II) reached 31.72, 80.52 and 95.11 mg/g, respectively while the maximum adsorption capacities for Pb(II) were 48.46, 134.26 and 164.08 mg/g, respectively. These results are highly in agreement with the changing trends of their specific surface area, functional group abundance and porosity shown in Table 3. In addition, it is found that the maximum adsorption capacity for Pb(II) by three types of adsorbents is higher than that for Cu(II). This might be because that the hydrated ionic radius of Pb(II) was smaller than that of Cu(II)[42], making it more competitive than Cu(II) during the adsorption process when co-existed.

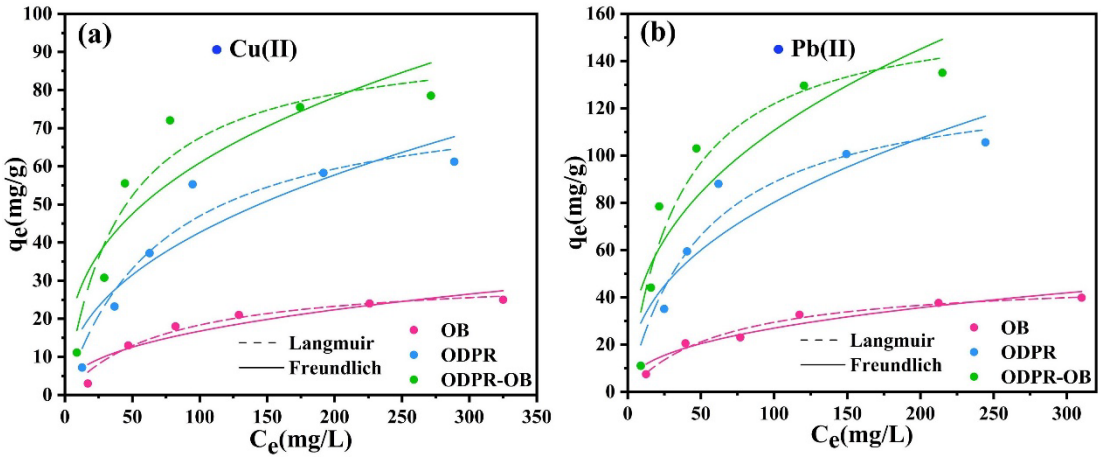

Fig. 11. Adsorption isotherms of Cu(II) (a) and Pb(II) (b) by OB, ODPR and ODPR-OB adsorbents at 25 ℃.

Table 3 Langmuir and Freundlich model parameters for Cu(II) and Pb(II) adsorption by OB, ODPR and ODPR-OB adsorbents, repsectively

Adsorbents	Adsorption isotherms	Parameters	Cu	Pb
OB	Langmuir	q_m	31.7239	48.45714
		k_L	0.01373	0.01548
		R_2	0.95557	0.9699

ODPR	Freundlich	k_F	2.45773	1.3968
		1/n	0.4167	0.06406
		R_2	0.83964	0.92174
	Langmuir	q_m	80.52421	134.25544
		k_L	0.01398	0.01946
		R_2	0.92549	0.93176
ODPR-OB	Freundlich	k_F	5.70086	6.1146
		1/n	0.43692	0.10814
		R_2	0.81141	0.81133
	Langmuir	q_m	95.11495	164.0803
		k_L	0.02439	0.02887
		R_2	0.91348	0.90212
	Freundlich	k_F	11.66784	9.27509
		1/n	0.35882	0.10822
		R_2	0.76103	0.7719

3.4 Competitive adsorption of Cu(II) and Pb(II) by adsorbents at different pHs

Statistical analysis was performed using AIC model to obtain the data in Figure 4. Table 4 shows that the selectivity of OB for Pb(II) was higher than that of Cu at all pH conditions, which was also consistent with the results of biochar preparation from peanut and chestnut shells in the literature [43]. However, the selectivity of OB and ODPR-OB to Pb(II) was higher than that of Cu(II) only when pH was greater than 3. These results indicated that electronegativity and hydrated ionic radius [44] affected the affinity and selectivity of Cu(II) and Pb(II) to adsorbents. Since Pb(II) had a smaller hydrated ionic radius and a larger electronegativity than Cu(II), OB had a better choice for Pb(II) than Cu(II). However, both ODPR and ODPR-OB functional groups could interact with Cu(II) and Pb(II), making them more inclined to adsorb Cu(II) at a lower pH. This also proved again that the ODPR-OB composite effectively retained the characteristic functional groups on ODPR.

Table 4 Competitive Binding Behavior of three Adsorbents to Cu(II) and Pb(II).

Adsorbents	pH-Cu(Pb)	k_d-Cu	α_1-Cu	k_d-Pb	α_2-Pb
OB	2	0.0276	0.7942	0.0347	1.2591
	3	0.0910	0.7820	0.1164	1.2788
	4	0.1233	0.6776	0.1820	1.4759
	5	0.2042	0.8166	0.2500	1.2246
	5.3(5.8)	0.2651	0.8331	0.3182	1.2004

Adsorbents	pH-Cu(Pb)	k_d-Cu	α_1-Cu	k_d-Pb	α_2-Pb
ODPR	2	0.0726	1.4017	0.0518	0.7134
	3	0.2074	0.8296	0.2500	1.2054
	4	0.2923	0.4169	0.7013	2.3989
	5	0.4286	0.3475	1.2331	2.8773
	5.3(5.8)	0.6640	0.4401	1.5087	2.2721
ODPR-OB	2	0.192	2.1226	0.0905	0.4711
	3	0.3909	1.1958	0.3269	0.8363
	4	0.5335	0.5595	0.9536	1.7874
	5	0.8519	0.3176	2.6822	3.1487
	5.3(5.8)	1.1277	0.2672	4.2199	3.7422

3.5 The comparison of ODPR-OB composite as adsorbents with others in literature for Cu(II) and Pb(II) removal from wastewater

Table 5 shows the comparison of different types of adsorbents developed for Cu(II) and Pb(II) removal from wastewater. It could be seen that the adsorption capacity of OB was similar to other adsorbents reported in the literature while the adsorption capacity of ODPR was significantly higher than other types of adsorbents, disclosing the potential of ODPR for use as adsorbents. By developing composite from OBDC and OP, the adsorption capacity was further increased. Given the fact that both OBDC and OP are wastes that need disposal, the composite developed from OBDC and OP has great potential for the practical application in Cu(II) and Pb(II) removal from industrial wastewater, particularly when it combines with fuel production from wastes with pyrolysis.

Table 5 Comparison of adsorption capacity of different materials for Cu(II) and Pb(II) removal from wastewater

Adsorbents	heavy metals	adsorption capacity (mg/g)	reference documentation
Modified carbon powder	Cu(II)	12	[45]
Turf	Pb(II)	82.3	[46]
Grass×Bamboo-derived biochar	Cu(II)	15.7	[11]
Clay, sawdust and peanut shells	Pb(II)	39	[7]
Lignite	Cu(II)	25.5	[47]
	Cu(II)	17.8	
	Pb(II)	56.7	
Farm and poultry manure biochar	Cu(II)	44.5	[10]

Adsorbents	heavy metals	adsorption capacity (mg/g)	reference documentation
Chestnut biochar	Pb(II)	8.5	[9]
	Cu(II)	5.5	
OB	Cu(II)	31.72	this research
	Pb(II)	48.46	this research
ODPR	Cu(II)	80.52	this research
	Pb(II)	134.26	this research
ODPR-OB	Cu(II)	95.11	this research
	Pb(II)	164.08	this research

4 Conclusions

The biochar composite developed from the mixture of two types of wastes, i.e., Oil-based drilling cuttings and orange peel at 1:1 ratio demonstrated much better adsorption performance than each individual adsorbent from OBDC or OP, respectively. This indicates that the biochar composite is not a simple mixture of each individual char from ODPR or OP. Instead, reaction and interaction occurred during the pyrolysis of the mixture of ODPR and OP for improved physicochemical properties as adsorbents for Cu(II) and Pb(II) removal. The adsorption kinetics of Cu(II) and Pb(II) by the ODPR-OB biochar composite could be described by the pseudo-second-order model while the adsorption isotherm behavior of Cu(II) and Pb(II) is in agreement with the Langmuir model. The synergistic effect enhanced the adsorption capacity of ODPR-OB composite, which has great potential for practical application to treat industrial wastewater for Cu(II) and Pb(II) removal given the fact that both OBDC and OP are wastes for disposal.

References:

1. Kumar, V., et al., *Global evaluation of heavy metal content in surface water bodies: A meta-analysis using heavy metal pollution indices and multivariate statistical analyses. %J Chemosphere.* 2019. **Vol.236**: p. 124364.
2. Zanina, E., et al., *Adsorption of heavy metals from wastewater graphic industry using clinoptilolite zeolite as adsorbent %J Process Safety and Environmental Protection.* 2017. **Vol.105**(Part B): p. 194-200.
3. Bolisetty, S., M. Peydayesh, and R. Mezzenga, *Sustainable technologies for water*

purification from heavy metals: review and analysis. %J Chemical Society reviews. 2019. **Vol.48**(No.2): p. 463-487.

4. Rai, P., et al., *Heavy metals in food crops: Health risks, fate, mechanisms, and management. %J Environment International.* 2019. **Vol.125**: p. 365-385.
5. Chen1, H., A. Xie2, and S. You3, *A Review: Advances on Absorption of Heavy Metals in the Waste Water by Biochar %J IOP Conference Series: Materials Science and Engineering.* 2018. **Vol.301**(No.1): p. 012160.
6. Zamora-Ledezma1CA1, C., et al., *Heavy metal water pollution: A fresh look about hazards, novel and conventional remediation methods %J Environmental Technology & Innovation.* 2021. **Vol.22**: p. 101504.
7. Mungondori, H.H., et al., *Synthesis and application of a ternary composite of clay, saw-dust and peanut husks in heavy metal adsorption %J Water Science and Technology.* 2017. **Vol.75**(No.9-10): p. 2443-2453.
8. Shehzad, K., et al., *Facile synthesis of novel calcined magnetic orange peel composites for efficient removal of arsenite through simultaneous oxidation and adsorption.* J Colloid Interface Sci, 2018. **511**: p. 155-164.
9. aacute, et al., *Chestnut shell as heavy metal adsorbent: Optimization study of lead, copper and zinc cations removal %J Journal of Hazardous Materials.* 2009. **Vol.172**(No.2-3): p. 1402-1414.
10. Batool, S., 2, et al., *Adsorption of copper (II) by using derived-farmyard and poultry manure biochars: Efficiency and mechanism %J Chemical Physics Letters*. 2017. **Vol.689**: p. 190-198.
11. Cibati, A., B. Foereid, and A. Bissessur, *Assessment of Miscanthus × giganteus derived biochar as copper and zinc adsorbent: Study of the effect of pyrolysis temperature, pH and hydrogen peroxide modification(Article) %J Journal of Cleaner Production.* 2017. **Vol.162**: p. 1285-1296.
12. Gao, R., et al., *Highly-effective removal of Pb by co-pyrolysis biochar derived from rape straw and orthophosphate.* J Hazard Mater, 2019. **371**: p. 191-197.
13. Ismadji, S., et al., *Bentonite hydrochar composite for removal of ammonium from Koi fish tank.* Applied Clay Science, 2016. **119**: p. 146-154.
14. Song, J., et al., *Preparation of montmorillonite modified biochar with various temperatures and their mechanism for Zn ion removal.* J Hazard Mater, 2020. **391**: p. 121692.
15. Rawal, A., et al., *Mineral-Biochar Composites: Molecular Structure and Porosity.* Environ Sci Technol, 2016. **50**(14): p. 7706-14.
16. Xu, X., et al., *Indispensable role of biochar-inherent mineral constituents in its environmental applications: A review.* Bioresour Technol, 2017. **241**: p. 887-899.
17. Liuyang, X., et al., *Resource utilization of secondary pyrolysis oil-based drilling cuttings ash for removing Cr (VI) contaminants: Adsorption properties, kinetics and mechanism.* Journal of Environmental Chemical Engineering, 2020. **8**(6).
18. Wu, C., et al., *Arsenic sorption by red mud-modified biochar produced from rice straw. %J Environmental Science & Pollution Research.* 2017. **Vol.24**(No.22): p. 18168-18178.
19. Azizian, S., S. Eris, and L.D. Wilson, *Re-evaluation of the century-old Langmuir isotherm for modeling adsorption phenomena in solution %J Chemical Physics.* 2018. **Vol.513**: p. 99-104.

20. Stromer, B.S., B. Woodbury, and C.F. Williams, *Tylosin sorption to diatomaceous earth described by Langmuir isotherm and Freundlich isotherm models. %J Chemosphere.* 2018. **Vol.193**: p. 912-920.
21. Moghaddam, M., S. Fatemi, and A. Keshtkar, *Adsorption of lead (Pb2+) and uranium (UO22+) cations by brown algae; experimental and thermodynamic modeling %J CHEMICAL ENGINEERING JOURNAL.* 2013. **Vol.231**: p. 294-303.
22. Ho, Y. and G. McKay, *The Kinetics of Sorption of Divalent Metal Ions onto Sphagnum Moss Flat %J Water Research.* 2000. **Vol.34**(No.3): p. 735-742.
23. Alam, S., et al., *Removal of Heavy Metals from Aqueous Solution by Adsorption on Biomass Based Adsorbent. %J TENSIDE SURFACTANTS DETERGENTS.* 2013. **Vol.50**(No.5): p. 346-359.
24. Chen, K., et al., *Facile synthesis of chitosan derived heteroatoms-doped hierarchical porous carbon for supercapacitors. %J Microporous & Mesoporous Materials.* 2021. **Vol.320**.
25. Tobi, A.R., et al., *Comparative analysis of physiochemical properties of physically activated carbon from palm bio-waste(Article) %J Journal of Materials Research and Technology.* 2019. **Vol.8**(No.5): p. 3688-3695.
26. Stepkowska, E.T., et al., *Thermo XRD-analysis of two aged cement pastes %J Journal of Thermal Analysis and Calorimetry.* 2005. **Vol.80**(No.1): p. 193-199.
27. Xiao, Y., et al., *Sorption of heavy metal ions onto crayfish shell biochar: Effect of pyrolysis temperature, pH and ionic strength.* Journal of the Taiwan Institute of Chemical Engineers, 2017. **80**: p. 114-121.
28. Reguyal, F., A.K. Sarmah, and W. Gao, *Synthesis of magnetic biochar from pine sawdust via oxidative hydrolysis of FeCl2 for the removal sulfamethoxazole from aqueous solution.* J Hazard Mater, 2017. **321**: p. 868-878.
29. Chao Ma1, et al., *Transfer of FeS-bound arsenic into pyrite during the transformation of amorphous FeS to pyrite %J Applied Geochemistry.* 2020. **Vol.119**: p. 104645.
30. Afolayan, D.O., dCAa, et al., *Characterization of barite reserves in Nigeria for use as weighting agent in drilling fluid %J Journal of Petroleum Exploration and Production.* 2021. **Vol.11**(No.5): p. 2157-2178.
31. Ahmad, M., 2, et al., *Biochar as a sorbent for contaminant management in soil and water: A review. %J Chemosphere.* 2014. **Vol.99**: p. 19-33.
32. Deng, C. and M. Zhu, *New Type Nitrogen-Doped Carbon Material Applied to Deep Adsorption Desulfurization.* Energy & Fuels, 2020. **34**(8): p. 9320-9327.
33. Tang, X., et al., *Extremely efficient and rapidly adsorb methylene blue using porous adsorbent prepared from waste paper: Kinetics and equilibrium studies.* J Hazard Mater, 2021. **402**: p. 123579.
34. Lu, H., et al., *Relative distribution of Pb2+ sorption mechanisms by sludge-derived biochar.* Water Res, 2012. **46**(3): p. 854-62.
35. Kruk, M. and M. Jaroniec, *Gas Adsorption Characterization of Ordered Organic-Inorganic Nanocomposite Materials %J Materials Chemistry.* 2001. **Vol.13**(No.10): p. 3169-3183.
36. Li, S., et al., *Mg/Al-layered double hydroxide modified biochar for simultaneous removal phosphate and nitrate from aqueous solution.* Environmental Technology & Innovation, 2021. **23**.

37. Bibi, S., et al., *Evaluation of industrial based adsorbents for simultaneous removal of arsenic and fluoride from drinking water %J Journal of Cleaner Production.* 2015. **Vol.87**(No.1): p. 882-896.
38. Anoop Krishnan, K., et al., *Evaluation of adsorption properties of sulphurised activated carbon for the effective and economically viable removal of Zn(II) from aqueous solutions. %J Ecotoxicology & Environmental Safety.* 2016. **Vol.124**: p. 418-425.
39. Bulgariu, D., 2 and L. Bulgariu, *Potential use of alkaline treated algae waste biomass as sustainable biosorbent for clean recovery of cadmium(II) from aqueous media: batch and column studies. %J Journal of Cleaner Production.* 2016. **Vol.112**(Part 5): p. 4525-4533.
40. Vilvanathan, S. and S. Shanthakumar, *Ni2+ and Co2+ adsorption using Tectona grandis biochar: kinetics, equilibrium and desorption studies %J Environmental Technology.* 2018. **Vol.39**(No.4): p. 464-478.
41. Tofan, L., et al., *Cobalt (II) removal from aqueous solutions by natural hemp fibers: Batch and fixed-bed column studies %J APPLIED SURFACE SCIENCE.* 2013. **Vol.285**(No.1): p. 33-39.
42. Hao, D. and Y. Liang, *Adsorption of Cu(2+), Cd(2+) and Pb(2+) in wastewater by modified chitosan hydrogel.* Environ Technol, 2022. **43**(6): p. 876-884.
43. Sun, J., et al., *Unravelling the adsorption disparity mechanism of heavy-metal ions on the biomass-derived hierarchically porous carbon %J Applied Surface Science.* 2019. **Vol.471**: p. 615-620.
44. Martin-Lara, M.A., G. Tenorio, and G. Blazquez, *Batch biosorption of lead(II) from aqueous solutions by olive tree pruning waste: Equilibrium, kinetics and thermodynamic study(Article) %J Chemical Engineering Journal.* 2011. **Vol.168**(No.1): p. 170-177.
45. Lee, C.-G., et al., *Removal of copper, nickel and chromium mixtures from metal plating wastewater by adsorption with modified carbon foam. %J Chemosphere.* 2017. **Vol.166**: p. 203-211.
46. Bartczak, P., et al., *Removal of nickel(II) and lead(II) ions from aqueous solution using peat as a low-cost adsorbent: A kinetic and equilibrium study(Article) %J Arabian Journal of Chemistry.* 2018. **Vol.11**(No.8): p. 1209-1222.
47. Pehlivan, E., Email:erolpehlivan@gmail.com, and G. Arslan, *Removal of metal ions using lignite in aqueous solution—Low cost biosorbents %J Fuel Processing Technology.* 2007. **Vol.88**(No.1): p. 99-106.